DEVELOPMENT OF A THREE-DIMENSIONAL VELOCITY MODEL FOR THE CRUST AND UPPER MANTLE IN THE GREATER BARENTS SEA REGION

Hilmar Bungum[1,2], Nils Maercklin[1], Oliver Ritzmann[2], Jan Inge Faleide[2,1], Christian Weidle[2], Anatoli Levshin[3], Johannes Schweitzer[1], Walter D. Mooney[4], and Shane T. Detweiler[4].

NORSAR[1], University of Oslo[2], University of Colorado[3], and United States Geological Service[4]

ABSTRACT

We have compiled a 3D seismic velocity model for the crust and upper mantle in the greater Barents Sea region including northern Scandinavia, Svalbard, Novaya Zemlya, the Kara Sea and the Kola-Karelia regions. While the general motivation for developing this model is basic geophysical research, a more specific goal is to create a model for research on the identification and location of small seismic events in the study region, and for operational use in locating and characterizing seismic events in the study region.

The observational basis for the velocity model are previous, crustal-scale 2D seismic reflection and refraction profiles, and passive seismological recordings, supplemented by potential field data to provide additional constraints on the crustal structure. The model is defined at grid tiles spaced every 50 km, and each tile is represented by up to two sedimentary and three crystalline crustal layers (plus water and ice). For crustal regions not constrained by primary velocity data, we developed an interpolation scheme based on several defined geological provinces that are characterized by individual tectono-sedimentary histories. The interpolation utilizes the observed strong correlation between sediment and crystalline crustal thickness within continental provinces. For comparison, an alternative interpolation approach applies a continuous curvature gridding algorithm within each of the provinces.

To provide a complete lithospheric model, we complemented the crustal model with an upper mantle velocity model based on surface wave inversion, thereby covering depths essential for P_n and S_n travel time modeling. As an extension to the previously existing data set, we recently retrieved a large amount of surface wave data recorded or excited in the European Arctic during the last three decades. The merged surface wave data set will enable us to refine the upper mantle velocity structure in the study region significantly. Preliminary group velocity maps for Rayleigh and Love waves reflect large-scale geological structures and demonstrate lateral velocity variations in the mantle.

Validation of our velocity model includes travel time modeling and relocation of seismic events. For this purpose we compiled a set of Ground Truth (GT) events comprising chemical and nuclear explosions, and natural earthquakes. Phase arrival times of multiple events at some sites provide timing error estimates at some stations. With the GT events we obtain a rather good P_n and S_n ray coverage in the main target region. Besides the comparison of observed and modeled travel times along selected transects, we have computed source-specific station corrections (SSSCs) from our 3D model.

The crustal velocity models are also evaluated by comparison of predicted gravity fields with the observed free-air gravity. To model the gravity field, we used standard velocity-density relationships for crustal rock types and the density structure of the upper mantle from previous studies. The inferred gravity fields both reflect and exaggerate the basic geological features. Accomplishments so far have been concerned with implementation of a forward modeling procedure and software development needed to support the complex 3D model structure. The forward modeling is done in order to reduce the misfit between observed and modeled gravity and finally to supplement our crustal velocity model with a density distribution.

OBJECTIVE

The principal objective of this study is to compile a 3D seismic velocity model of the crust and upper mantle for the Barents Sea, Novaya Zemlya, Kara Sea and Kola-Karelia regions (see Figure 1). The general motivation for developing this higher-resolution model is basic geophysical research as well as seismic verification. The goal is to provide a model useful both for further research on the detection, location and identification of small events in the study region, and for operational use in locating and characterizing seismic events in the region including event discrimination for nuclear test monitoring. Along with the development of the model, a calibration and validation program is executed, aimed both at quality controlling the model through comparisons between observed and synthetic travel times, and at investigating the potential improvements in terms of event locations.

RESEARCH ACCOMPLISHED

The observational basis for the velocity model are previous, crustal-scale 2D seismic reflection and refraction profiles, and passive seismological recordings, supplemented by potential field data to provide additional constraints on the crustal structure. The model is defined at grid tiles spaced every 50 km, and each tile is represented by up to two sedimentary and up to three crystalline crustal layers, plus water and ice (Bungum et al., 2004, 2005). Mantle velocities are described as continuous velocity-depth profiles at each tile.

For crustal regions not constrained by primary velocity data we developed two interpolation methods and currently evaluate both resulting models. The first utilizes sediment-to-total crustal thickness relationships to infer Moho-depth, hereafter called *db* (depth-to-basement) model, while the second model is constructed by continuous curvature gridding of the Moho-depth entries of our compiled database, called *sg* (surface gridding) model. Both models are still under evaluation (see section on density modeling), and a decision a decision on which model to use for the final 3D model has not been made. Generally we would like to keep both models open for updates and new database entries. As an example, Figure 1 shows the Moho depths determined for the target area, based on the *db* interpolation scheme, and with an equal spaced grid with a node distance of 50 km. Due to a limited extension of the used depth-to-basement map, fundamental for this model, the Moho map terminates at 80.5°N.
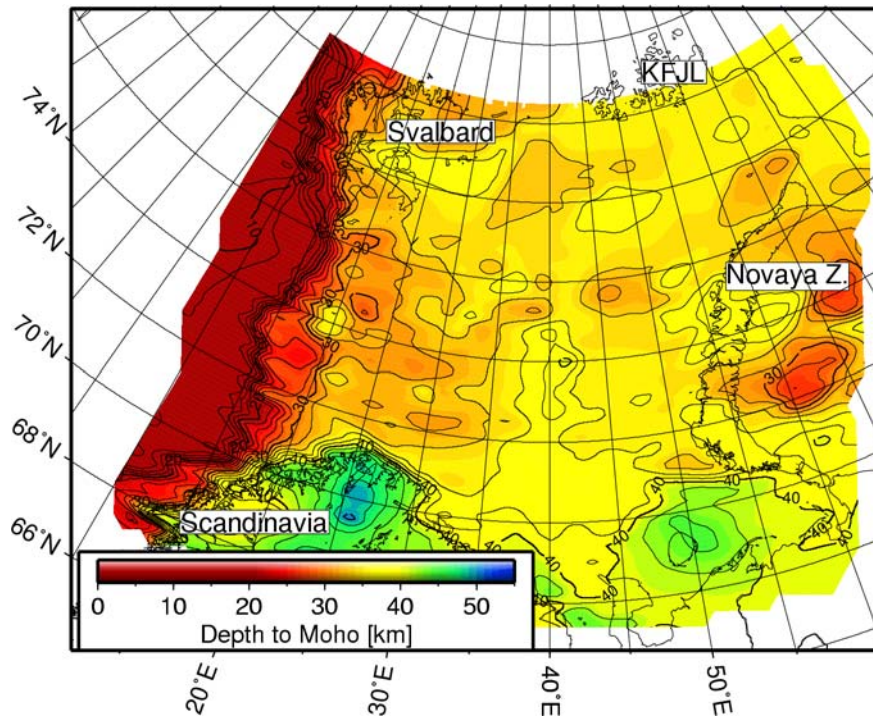

Figure 1.
Moho depth map for the main target area in the greater Barents Sea region. The depths are taken from the crustal model based on thickness relations (the so-called *db* model), and the contour interval is 2 km. KFJL, Kaiser Franz Josef Land.

The *db* interpolation method described above produces a consistent and smooth model that relates to the local extensional tectonic setting, but it does not completely preserve velocity and layer thickness data at constrained tiles. Therefore, as an alternative interpolation method, we also applied horizontal continuous curvature gridding of velocities and layer thicknesses within each of the geologic provinces (*sg* model).

To provide a complete lithospheric model, we complemented the crustal models with an upper mantle velocity structure derived from surface wave dispersion data (Shapiro & Ritzwoller, 2002), thereby covering depths sufficient for tracing far-regional wave paths. An ongoing study uses an extended surface wave data set to refine the upper mantle structure significantly.

Surface wave tomography

Existing global and regional tomographic models have limited resolution in the European Arctic due to the small number of seismic stations, low regional seismicity, and limited knowledge of the crustal structure. More recently, however, more seismic stations have been, permanently or temporarily, installed in and around this region. Many of these new recordings are, however, not accessible via the international data centers but only by direct request to the different station operators.

In this part of the project, we have extensively searched for larger events with observable surface wave radiation that occurred in or around the area of interest. Searching back to the early 1970s, we were able to retrieve Rayleigh and Love wave observations from the data archives at NORSAR, University of Bergen, University of Helsinki, the Kola Science Center in Apatity, the Geological Survey of Denmark, and the data centers IRIS and GEOFON. In these data archives, not yet analyzed Rayleigh- or Love-wave data were found for more than 200 seismic events (earthquakes and nuclear explosions). From these records group velocities of Rayleigh and Love waves were measured in the period range 10-150 s using the package for Frequency-Time Analysis developed at the University of Colorado (Ritzwoller & Levshin, 1998). After several cleaning procedures, the new measurements were combined with the existing set of group velocity measurements provided by the Center for Imaging the Earth's Interior at the Colorado University (CU; see Levshin et al., 2001). Only paths completely inside the cell [50-90°N, 60°W-60°E] were selected, such that the entire data set consists of paths within the same regional frame.

To demonstrate the amount of new surface wave observations, we compare in Table 1 the number of newly analyzed Rayleigh and Love wave observations with the number of the preselected set of data from University of Colorado (CU) that generously were made available to the project. Obviously, the new data set increased ray density and consequently the resolution of the planned tomography. In particular for short period data, the number of rays crossing the target area was increased by more than 200% for Rayleigh waves and close to 200% for Love waves. For longer periods (i. e., T > 80 s), the ratio of added data significantly drops since large seismic events, necessary to generate long period radiation, are very rare in this region.

All group velocity observations were inverted into group velocity maps (Barmin et al., 2001). In all cases, we inverted the combined data set of newly acquired and analyzed data and preselected CU data. From the cluster analysis (Ritzwoller and Levshin, 1998) the rms of the group velocity measurements in the considered period range for the new data set was estimated as 0.010-0.015 km/s for Rayleigh waves and 0.015-0.025 km/s for Love waves. As a first result, we present in Figure 2 group velocity maps for Rayleigh waves at three different periods: 16, 25, and 40 s. To illustrate the newly achieved, high path density, we also present in Figure 2 all paths of the newly acquired data set for respective periods. The Rayleigh wave group velocity maps (right panels), derived from the combined data base, show the lateral deviation of the group velocities from the average velocity in percent. Note that these deviations are up to ±36% for Rayleigh waves with a period of 16 s. This reflects the strong lateral heterogeneity of the Earth's crust in this region, which changes between the mid-oceanic ridge system (white line on the map), thick sedimentary basins in the Barents Sea, and old continental shields.

The next step will be the inversion of all group velocity maps (Love and Rayleigh waves) into a 3D shear velocity model for the whole region (Shapiro & Ritzwoller, 2002). As additional constraints the thickness of the sedimentary layer and the Moho depth, as they are derived during this project (Figure 1) will be included in the inversion. The result should yield a new, robust 3D model of the velocities in the upper mantle beneath the greater Barents Sea region down to about 100 km.

Table 1: Number of newly analyzed regional Rayleigh and Love wave observations with respect to their signal periods, compared to the initial data base made available from the University of Colorado (CU).

Period [s]	Rayleigh Waves			Love Waves		
	Number of New Data	Total Number of Data	Data Increase [%]	Number of New Data	Total Number of Data	Data Increase [%]
14	773	1072	259	354	546	184
16	1073	1526	237	529	802	194
18	1313	1898	224	635	958	197
20	1453	2124	217	687	1064	182
25	1642	2447	204	733	1184	163
30	1655	2488	199	697	1206	137
35	1522	2342	186	626	1119	127
40	1343	2138	169	508	971	110
45	1115	1863	149	397	823	93
50	953	1656	136	295	672	78
60	625	1245	101	154	461	50
70	384	925	71	64	289	28
80	211	684	45	36	194	23
90	106	509	26	25	138	22
100	81	425	24	11	80	16
125-200	50	548	10	6	59	11

Ground truth events

Validation of our velocity model includes forward modeling of observed body wave travel times and relocation of seismic events. For this purpose we compiled a set of reference events with known or well-located epicenters, referred to as Ground Truth (GT) events. Bungum et al. (2004) showed an initial set of potential GT events in the greater Barents Sea region comprising mainly natural events, but also some presumed mining explosions in northern Fennoscandia and on the Kola peninsula. Most of these events were used in studies by Hicks et al. (2004), and they are plotted as circles in Figure 3. The color-code of each event corresponds to the area of the respective location error ellipse using a 1D regional velocity model (BAREY; Schweitzer & Kennett, 2002).

We extended the initial database with reference events published by Bondár et al. (2004). All events in this database are classified already into GT levels, where GT*X* denotes *X* km maximum location error. Selected events from this database are plotted in Figure 3 with a color-code corresponding to the assigned GT level. These events comprise nuclear explosions in northwestern Russia and Novaya Zemlya (all red stars) as well as mining explosions and calibration shots in Fennoscandia and Kola. Besides events and stations, Figure 3 shows also all available P wave travel paths. The distribution of available S wave paths is only slightly poorer.

Although the majority of events collected at NORSAR (circles in Figure 3) have rather small location errors, many of these events would not pass formal GT*X* acceptance criteria (see e.g. Bondár et al., 2004). This is mainly due to the poor station coverage in the region, resulting often in a rather large maximum azimuthal gap, and the lack of a sufficient number of short-distance observations. However, seismic array recordings were used here, which provide additional constraints (azimuth and slowness) for the event location.

To get an estimate for timing of phase reading errors of events taken from Bondár et al. (2004), we have analyzed the consistency of travel times from many events at the same site. For example, station KHE (Kaiser Franz Josef Land; see Figure 3) recorded several of the Soviet nuclear explosions classified as GT1. Especially in this rather poorly constrained model region, accurate timing is mandatory for both the origin times and the arrival times at the station. Theoretically, the travel times of all recorded nuclear tests on the same site on Novaya Zemlya should be the same, but in fact, excluding outliers, we observe a scatter of about 2 s around the mean, i.e. the scatter is in the same range as the travel time residuals of our 3D model relative to a 1D regional model. The same observation applies to station KBS on Svalbard. Since the observed travel times from exactly the same events scatter much less (less than 0.5 s) at the stations APA and KEV (Kola peninsula), both in a similar distance range from the source as KHE and KBS, we conclude that the time variations are related to the stations. Taking a mean travel time at those stations might be most appropriate when comparing observed and modeled times.
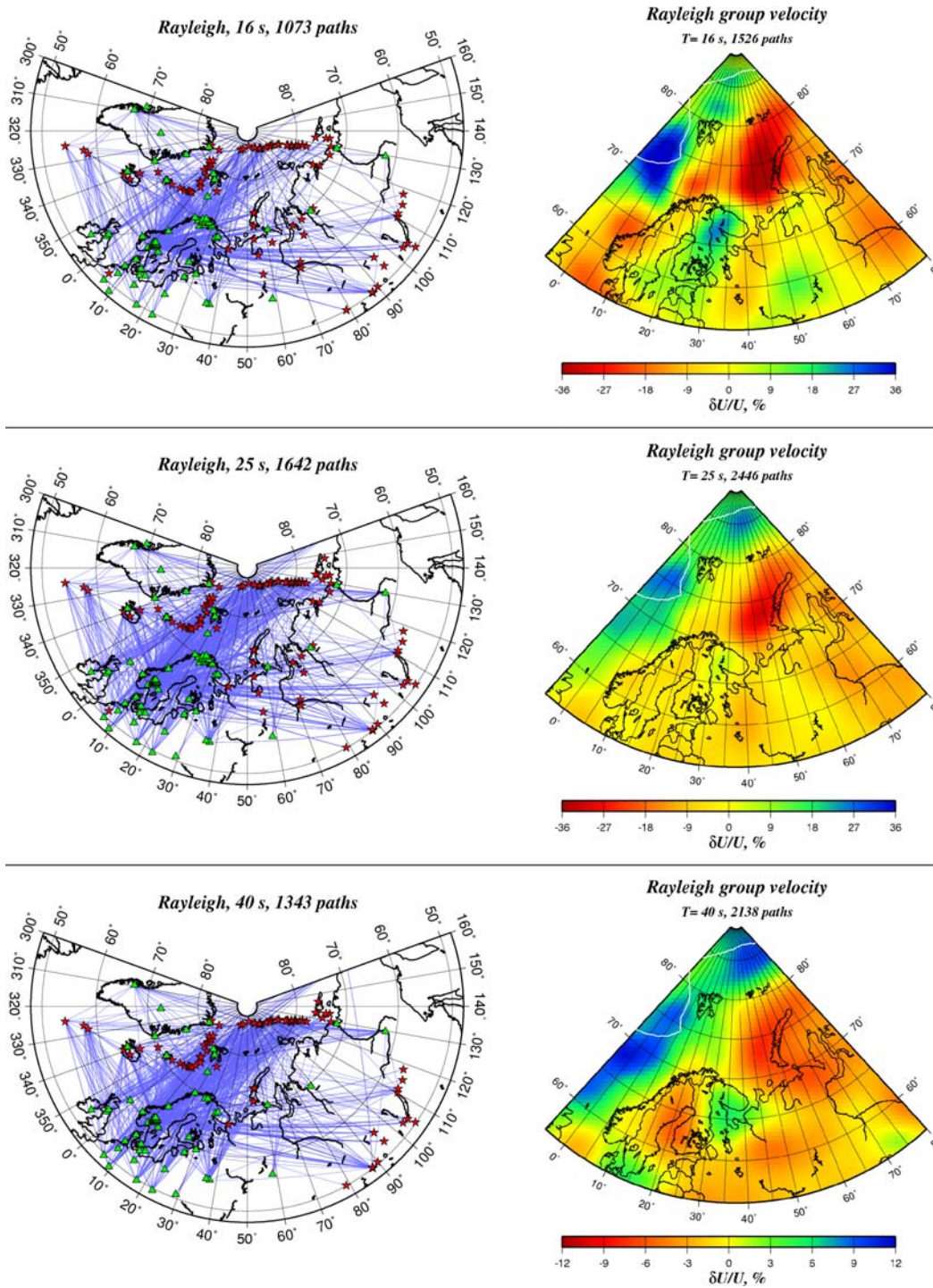
Figure 2. Ray paths (left) of newly analyzed Rayleigh waves (stations as green triangles, events as red stars), and the group velocities inverted with the whole data set (right), including also the initial data base from University of Colorado (CU), for different signal periods.
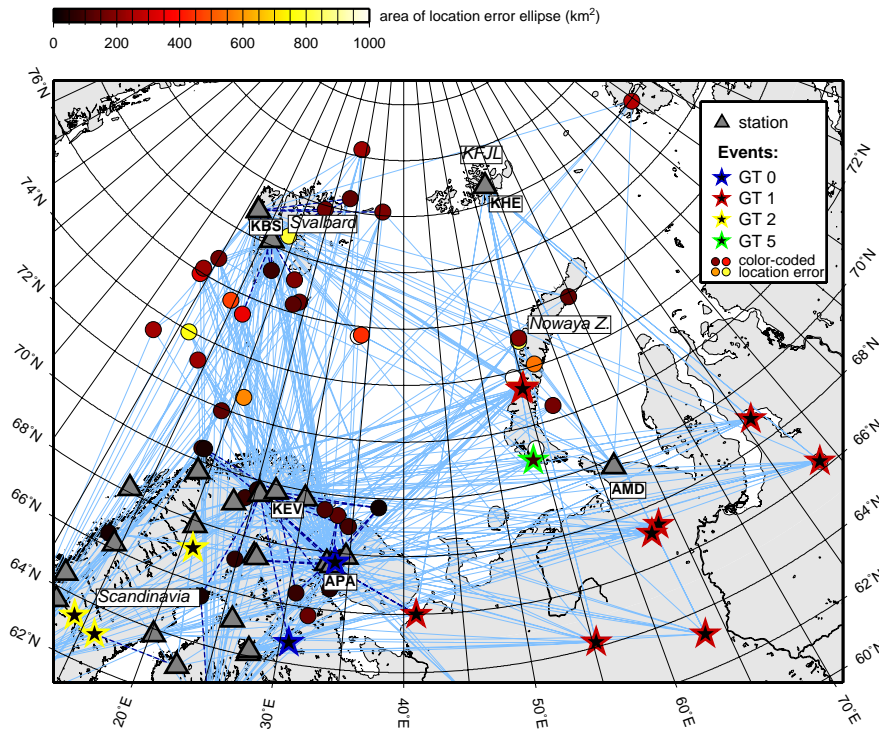
Figure 3.
Ground Truth events (circles, stars), seismic stations (triangles), and P_n (light blue) and P_g (dark blue, dashed) travel paths. Events collected at NORSAR are shown as circles with color-coded location error (Hicks et al., 2004; see also Bungum et al., 2004), whereas the events taken from Bondár et al. (2004) are plotted as stars with colors indicating their respective GT levels. The black circle near 69.6°N. 37.6°E is the Kursk explosion on August 12, 2000.
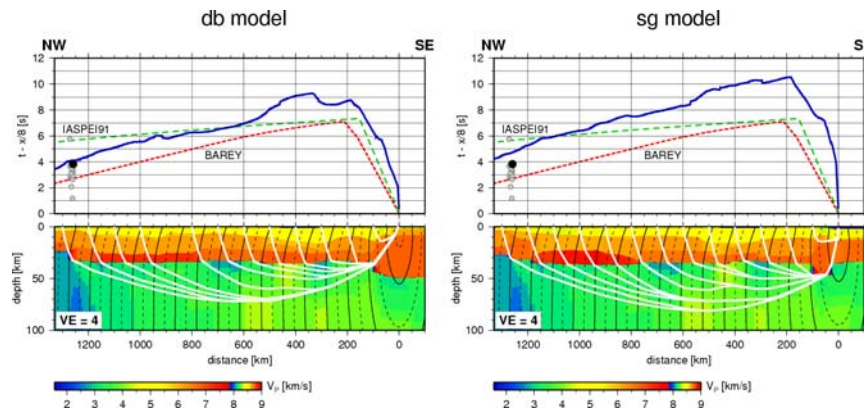

Figure 4.
Velocity transects from central Novaya Zemlya to station KBS (Svalbard) with superimposed rays (white) and wave fronts (solid black, spaced every 10 s). The interpolation method used to construct the crustal model is given at the top. Dashed travel time curves (top panels) correspond to 1D reference models, and the solid blue curve to the respective 3D model.

Figure 4 compares both crustal velocity models, i.e. the *db* model based on thickness relations (left) and the *sg* model from surface gridding (right), in terms of travel times. The example transect extends from the NZ test site mentioned above to the station KBS on Svalbard (Figure 3). The observed P_n travel times recorded at KBS (circles) are shown together with the calculated travel times continuously along the transect for both of our 3D models and the 1D reference models (IASPEI91 and BAREY). The average slope of the mantle phases of the travel time curves of our models and the BAREY model are very similar, according to similar upper mantle seismic velocities. On the other hand, our models reveal a nearly constant offset, i.e. later arrivals, compared to the 1D model. And moreover, small and local undulations along the P_n travel time curves show the regional differences between our two models (note profile section between km 200 and 400) and between our models and the reference models.

The case study shown in Figure 4 illustrates two issues: Firstly, it exemplifies the regional sensitivity of our compiled crustal models (not mantle) compared to the simple(r) 1D models. Not only large sedimentary basin structures (km 300) cause significant travel time delays but also local jumps in basement topography may result in 500 ms delay (km

950). Secondly, the absolute travel time between the source and the receiver may be modeled with a good fit, but the relevant elements for this calculation are the crustal columns below the source and receiver and the upper mantle model. Thus forward travel time modeling is confined to the limited amount of recorded events and the mantle structure along the path. Travel time modeling with the entire set of events derives a mean fit to all recorded travel times. The comparison between both models (*db*, *sg*) will most probably derive the more suitable model for fitting the recent set of recorded events.

Density modeling

Density modeling provides two important results that may be applied to the present velocity model. Firstly, it derives the requested density structure which is essential for later seismic wave field modeling using FE or FD techniques to study e.g. source characteristics. Secondly, density modeling works as a test for both models, since we can compare and link the induced gravity fields to the observed gravity. Further, software was developed using a grid search method in order determine the density field that fits best the observed gravity field. The final relationship between seismic velocity and density reveals basic physical rock properties and allows further discrimination of rock types and sheds lights on the geological evolution.

1. Getting the density structure from the seismic velocity field.

In order to derive an initial density model from the compiled seismic velocity models relationships established by Birch (1961) and Nafe & Drake (1957) for sedimentary rocks and Christensen & Mooney (1995) for continental crystalline rocks were used for conversion. Seismic wave velocity in an isotropic medium depends firstly on the atomic mass and material density, and secondly (in real rock formations) also on the given p/T field. Therefore, the results of the referred authors show a significant scatter around the mean density value for any crustal rocks. The scatter decreases with increasing seismic observation wavelengths which is almost large in the included crustal studies. Our chosen model construction shows (up to five) major crustal levels, or regional geological units so that we expect to narrow the scatter of possible densities significantly. The mean density for sedimentary rocks is taken from Barton's (1986) review of the earlier publications. The non-linear velocity-density regressions of Christensen & Mooney (1995) were utilized to infer a depth-dependent density field for crystalline rocks with respect to an underlying mantle.

2. Comparison of the theoretical and observed gravity fields

The calculation of the induced gravity of an arbitrarily shaped 3D body is rather complex and involves volume integration. We have taken into account the fact that our seismic velocity models are too complex in terms of the total number of bodies at the 1330/1490 nodes (the *db* and *sg* interpolation schemes, respectively). Every node bears a combination of a water layer, up to 5 crustal bodies and up to 35 mantle levels (Shapiro & Ritzwoller, 2002) depending on the desired depth of the density model. As the gravity field above a single grid node is influenced by all masses (or bodies) in the surrounding of the observation point, the local gravity field becomes a stack of contributions from all surrounding bodies. These bodies are rectangular shaped prisms on an equal-spaced grid. Therefore, we used Plouff's (1976) derivation of the integration term for a single rectangular prism, i.e. the summation of the responses from all corners of the prism multiplied by the prism density and gravity constant. In Figure 6 we present a calculation that incorporates the gravity effect of the 50x50 km wide bodies below the observation point, considered to be a good first approximation to the complete field inferred from all bodies of the model.
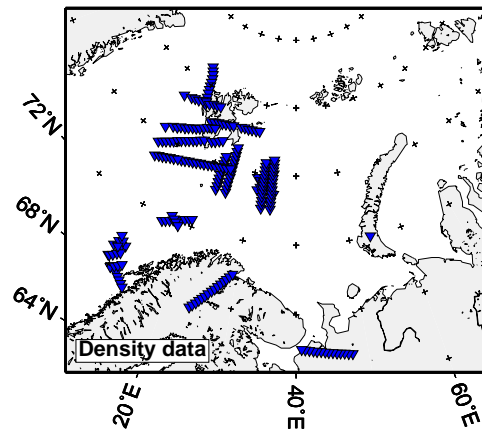

Figure 5. Location map of 2D wide-angle seismic transects in the Barents Sea region for which crustal densities have been modeled using measured layer boundaries and P wave velocities.

Local studies of the density structure along 2D seismic velocity transects are only available from modern OBS experiments (Figure 5). The data distribution is too insufficient to construct an independent density model from the data-

base as it was accomplished for seismic velocities. In order to built a uniform density model these results were not entered in the initial converted model. The density distribution of the upper mantle is given by the surface wave model of Shapiro & Ritzwoller (2002). The mantle density structure is kept fixed during all subsequent modeling steps.
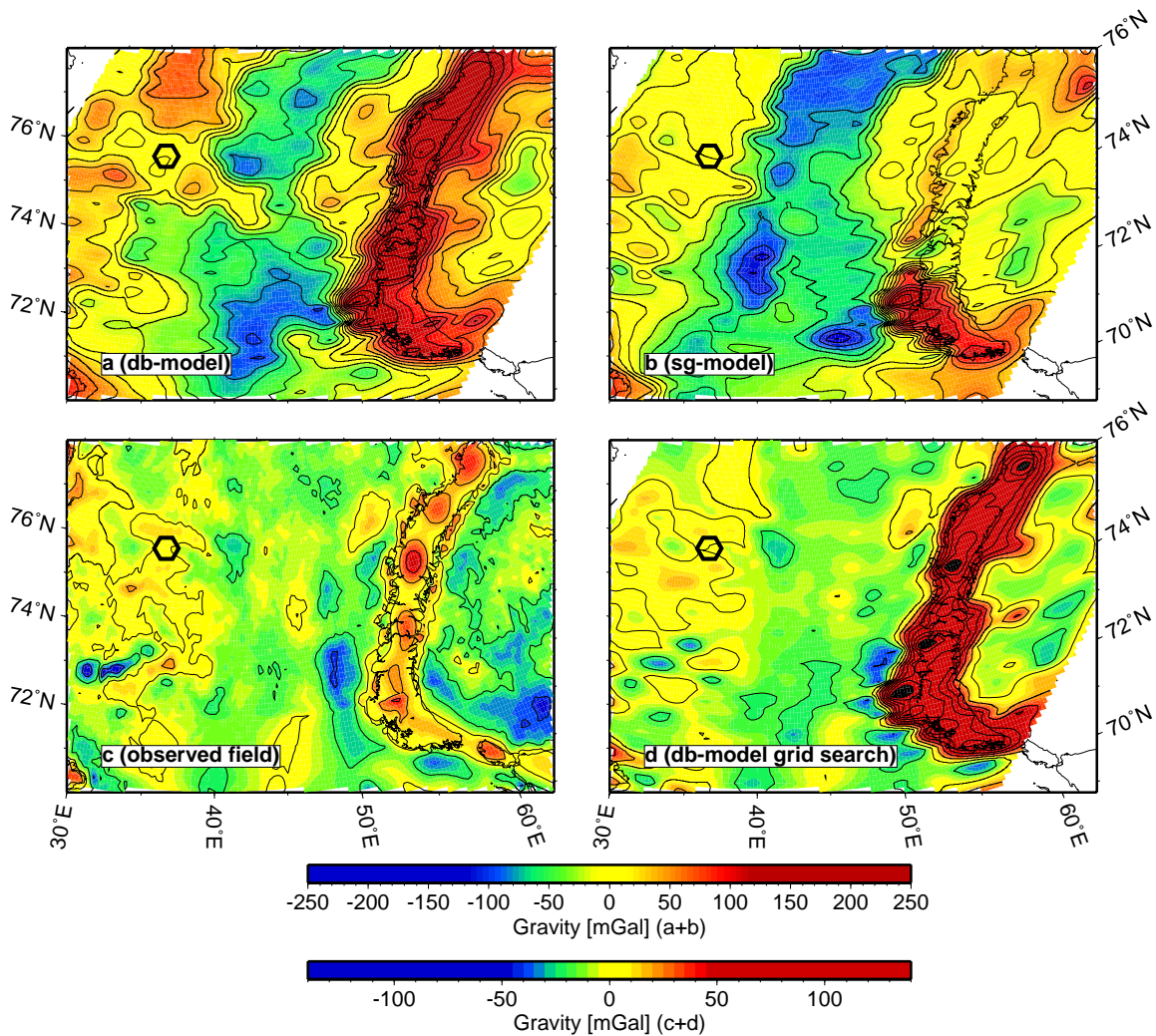

Figure 6. Density modeling results. (a) Gravity field inferred from the recent version of model *db*. (b) Gravity field inferred from the recent *sg* model. The lower gravity in northern Novaya Zemlya in (b) is due to the connection of the thick sedimentary sections in the Barents- and Kara Seas across Novaya Zemlya. (c) Observed gravity field (taken from Arctic Gravity Project, 2002). Note the different color scales for a/b and c/d. The black hexagon marks the reference location used for tying the calculated gravity fields (free-air anomaly = 0 mgal). (d) Gravity field inferred from the recent version of model *db* after applying the grid search algorithm to upper and lower sediment densities (partly also upper crystalline crust). West of Novaya Zemlya a good match to the observed field (c) could be achieved. To enhance the match on Novaya Zemlya and the Kara Sea, the grid search has to be extended to crystalline crustal rocks.

Figures 6a and 6b shows the calculated fields for the models *db* and *sg*, respectively. A major difference between the gravity effects of the models occurs in the northern part of Novaya Zemlya (NZ). The depth-to-basement compilation shows only a thin sedimentary cover onshore NZ. Therefore the shallow, higher-density crystalline rocks contribute significantly to the gravity field. The second model (b) is derived by surface gridding and shows a considerably lower gravity field across northern NZ. Thick sedimentary sections occur on both sides of NZ in the Barents and Kara Seas and are interpolated across NZ; an advantage of *db* model is that incorporates depth-to-basement information. The *sg* model shows more extreme values within the eastern Barents Sea sedimentary basins (blue shade). Both models

exaggerate the basic geological features, such as sedimentary basins or basement horsts. Interestingly these structures are well defined by analyzing regional seismic data of the region but have no pronounced expression in the observed field (Figure 6c).

3. Forward modeling (grid search) of the density structure

The gravity fields shown in Figure 6a and 6b clearly image the geological units that are present in the model region or, the depth-to-basement relief while the observed field is rather smooth. As mentioned earlier, the velocity-density relations used for model conversion all show a significant spread around the mean value taken here. The velocity of a single layer of a grid node is a mean velocity: during the calculation all compatible layers stored in the database (sediments or crystalline crust; seismic velocity above, between or below given thresholds) are used to stack the one-way travel times and the thicknesses of these layers to infer the seismic velocity for a single final model layer. This sustains the one-way travel times of the input models. Since the range of seismic velocities of crystalline crustal rocks in the continental domain is narrow, the mean seismic velocity is very close to all of the input layer velocities. Instead, the bandwidth of velocity of sedimentary rocks is very large and may range from 3.0-6.5 (7.0?) km/s for the lower sediments. Thus, the mean velocities have large standard deviations ($\sigma<0.67$). We expect therefore the velocity-density conversion for the upper and lower sedimentary layers to be a likely cause of the mismatches to the observed gravity field, because a series of layers with different densities and depths (or distances to an observation point) is 'gathered' to a single prism in the model.

We therefore programmed a grid search algorithm to adjust the densities of the upper and lower sediment within a given uncertainty range. According to Barton's (1986) review the spread in density increases drastically towards low seismic velocities (±0.3 g/cm^3) and is moderate to low within rocks of higher velocity (±0.1-0.2 g/cm^3). Therefore the grid search is limited to a maximum deviation of ±0.2 g/cm^3 for upper sediments and ±0.13 g/cm^3 for lower sediments (~60%). The search is further performed from the top to the bottom layers (upper, lower sediment, upper crystalline crust etc.) until a reasonable fit to the observed gravity is given. Due to our regional study of the crust and mantle a residual of ±5 mgal is regarded as a good fit. As some provinces do not reveal both upper and lower sediments, the underlying crystalline layers were altered to obtain a good fit. Figure 6d shows the gravity field inferred by the adjusted 'db' model. A good fit is achieved compared to the observed field (Figure 6c), disregarding Novaya Zemlya where no thicker sediment layers are present. Although the gravity field is inferred only from model prisms directly below, clear trends in the grid search are observed. For example, sediment densities in the eastern Barents Basin are obviously too low and were increased after the grid search. This result fits to the enormous depths of these basins (up to 20 km) which may result in high compaction and the increase of the regional density. Future work will include the comparison between the adjusted models, *db* and *sg*, respectively. The magnitude of necessary adjustments might be an indicator for the quality of the input velocity model.

CONCLUSIONS AND RECOMMENDATIONS

At this stage, when we are well into the second year of this two-year study, the 50x50 km 3D model for the crust in the greater Barents Sea region is in the final stages of preparation. We have, however, developed this model through two different approaches for interpolation in areas with less primary data coverage, namely (1) an interpolation scheme using geological background information, i.e. depth-to-basement (*db*) data outside data base information, and (2) an interpolation scheme (called *sg*) using a full mathematical approach, i.e. continuous curvature or surface gridding (*sg*) of data base information. The two approaches give results that differ only at a more detailed level, but since the question of which one to use is methodologically interesting they will both for some time continue to be evaluated against new data. To this end the density modeling work reported on here has been essential, since this allows us to compare and link the induced gravity fields from the two models to the observed gravity. However, at the end of the project only one model will be presented as the 'final' one.

Since last year (Bungum et al., 2004) significant developments have been achieved also in terms of an improved upper mantle model. Large amounts of new 10-150 s surface wave (Rayleigh and Love) data have been collected and analyzed, improving in particular the regional coverage in the lower period ranges. The group velocity observations have been inverted into group velocity maps, combining new and old data. The next step will be to invert the Rayleigh and Love wave group velocities into a 3D shear velocity model for the greater Barents Sea region, constrained

by the already established Moho depths and crustal velocities. This will cover depths down to about 100 km and thereby also many of the regional S_n and P_n ray paths essential for improved event locations.

In order to evaluate the potential event location improvements from the new 3D model we have also established a new data base of (GT) events in the region. However, since the availability of recording stations has been limited, many of these events would not pass formal GT acceptance criteria. Our analysis has also shown that there are timing errors on some of the stations that have recorded the earlier nuclear explosions from Novaya Zemlya. Even so, essential comparisons between observed and computed travel times have already been conducted.

<u>REFERENCES</u>

Barmin, M. P., M. H. Ritzwoller, and A. L. Levshin (2001), A fast and reliable method for surface wave tomography, *Pure Appl. Geophys.* 158: 1351-1375.

Barton, P. J. (1986), Comparision of deep reflection and refraction studies in the North Sea, in Barazangi, M. and L. D. Brown (eds.), Reflection seismology; a global perspective, *Geodynamic Series* 13: 297-300.

Birch, F. (1961), The velocity of compressional waves in rocks to 10 kilobars (Part II), *J. Geophys. Res.* 66: 2199-2224.

Bondár, I, E. R. Engdahl, X. Yang, H. A. A. Ghalib, A. Hofstetter, V. Kirichenko, R. Wagner, I. Gupta, G. Ekström, E. Bergman, H. Israelsson, and K. McLaughin (2004), Collection of a reference event set for regional and teleseismic calibration, *Bull. Seis. Soc. Am.* 94: 1528–1545.

Bungum, H., O. Ritzmann, N. Maercklin, J. I. Faleide, W. D. Mooney, and S. T. Detweiler (2005), Three-dimensional model for the crust and upper mantle in the Barents Sea region, in *Eos. Trans. Am Geophys. Union*, 86: 160–161.

Bungum, H., O. Ritzmann, J. I. Faleide, N. Maercklin, J. Schweitzer, W. D. Mooney, S. T. Detweiler, and W. S. Leith (2004), Development of a three-dimensional velocity model for the crust and upper mantle in the Barents Sea, Novaya Zemlya and Kola-Karelia regions, in *Proceedings of the 26th Seismic Research Review: Trends in Nuclear Explosion Monitoring*, Vol. 1, pp. 50-60.

Christensen, N. I. and W. D. Mooney (1995), Seismic velocity structure and composition of the continental crust: A global view, *J. Geophys. Res.* 100: 9761-9788.

Hicks, E. C., T. Kværna, S. Mykkeltveit, J. Schweitzer, and F. Ringdal (2004), Travel-times and attenuation relations for regional phases in the Barents Sea region, *Pure Appl. Geophys.* 161: 1–19.

Levshin, A. L., M. H. Ritzwoller, M. P. Barmin, A. Villaseñor, and C. A. Padgett (2001), New constraints on the arctic crust and uppermost mantle: surface wave group velocities, P_n, and S_n, *Phys. Earth Planet. Int.*, 123: 185-204.

Nafe, J. E. and C. L. Drake (1957), Variation with depth in shallow and deep water marine sediments of porosity, density and velocities of compressional- and shear waves, *Geophysics*, 22(3): 523-552.

Plouff, D. (1976), Gravity and magnetic fields of polygonal prisms and application to magnetic terrain corrections, *Geophysics* 41: 727-741.

Ritzwoller, M. H. and A. L. Levshin (1998), Eurasian surface wave tomography: Group velocities, *J. Geophys. Res.* 103: 4839-4878.

Schweitzer, J. and B.L.N. Kennett (2002), Comparison of location procedures – The Kara Sea event of 16 August 1997, Semiannual Technical Summary, NORSAR Sci. Rep., No. 1-2002, Kjeller, Norway.

Shapiro, N. M. and M. H. Ritzwoller (2002), Monte-Carlo inversion for a global shear velocity model of the crust and upper mantle, *Geophys. J. Int.* 151: 88-105.